Unified first-principles theory of thermal properties of insulators

Navaneetha K. Ravichandran and David Broido

Phys. Rev. B **98**, 085205 — Published 13 August 2018

DOI: 10.1103/PhysRevB.98.085205

Unified first-principles theory of thermal properties of insulators

Navaneetha K. Ravichandran and David Broido*

Department of Physics, Boston College, Chestnut Hill, MA 02467, USA

Abstract

The conventional first-principles theory for the thermal and thermodynamic properties of insulators is based on the perturbative treatment of the anharmonicity of crystal bonds. While this theory has been a successful predictive tool for strongly-bonded solids such as diamond and silicon, here we show that it fails dramatically for strongly anharmonic (weakly-bonded) materials, and that the conventional quasi-particle picture breaks down at relatively low temperatures. To address this failure, we present a unified first-principles theory of the thermodynamic and thermal properties of insulators that captures multiple thermal properties within the same framework across the full range of anharmonicity from strongly-bonded to weakly-bonded insulators. This theory features a new phonon renormalization approach derived from many-body physics that creates well-defined quasi-particles even at relatively high temperatures, and it accurately captures the effects of strongly anharmonic bonds on phonons and thermal transport. Using a prototypical strongly anharmonic material - sodium chloride (NaCl) as an example, we demonstrate that our new first-principles framework *simultaneously* captures the apparently contradictory experimental observations of large thermal expansion and low thermal conductivity of NaCl on the one hand, and anomalously weak temperature dependence of phonon modes on the other, while the conventional theory fails in all three cases. We demonstrate that four-phonon scattering due to higher-order anharmonicity significantly lowers the thermal conductivity of NaCl and is required for a proper comparison to experiment. Furthermore, we show that our renormalization framework, along with four-phonon scattering, also successfully predicts the measured phonon frequencies and thermal properties of a weakly anharmonic material - diamond, indicating universal applicability for thermal properties of insulators. Our work gives new insights into the physics of heat flow in solids, and presents a computationally efficient and rigorous framework that captures the thermal and thermodynamic properties of both weakly and strongly-bonded insulators simultaneously.

* broido@bc.edu

I. INTRODUCTION

Phonons, which are collective vibrations of a crystal lattice, are the primary energy carriers in semiconductors and insulators. The anharmonicity of inter-atomic bonds in these solids plays a fundamental role in several phonon-driven phenomena such as structural phase transitions, thermal expansion and resistance to heat flow. Understanding phonon thermodynamics and thermal transport in materials with strongly anharmonic bonds has been a topic of intense research interest among the solid-state physics, materials science, chemistry and geology communities due to the ubiquitous presence of such materials and their technological importance. For example, materials that are strongly anharmonic even at room temperature, like heavy-metal chalcogenides and complex metallic hydrides, make excellent thermal insulators, thermoelectric modules [1] and energy storage devices [2], and anharmonic materials like alkaline-earth oxides in the earth's core and mantle operate at high pressure and temperature [3], and drive the geological changes occurring underneath the earth's surface.

While it has been possible to experimentally measure macroscale collective phonon properties such as thermal expansion and thermal conductivity of insulators for more than a century, the recent advances in experimental techniques such as inelastic neutron scattering (INS) [4, 5] and transient grating spectroscopy [6] have now enabled accurate measurements of microscopic phonon-specific properties such as phonon dispersions and mean free paths. Theoretical treatment of phonon properties, both for predicting new thermal phenomena and for understanding novel observations of the aforementioned experiments, has evolved from simple models [7, 8] to more sophisticated first-principles quantum mechanical treatments of phonons and thermal properties in solids over the past few decades [9–15]. These conventional first-principles methodologies, which are built on the lowest-order perturbative treatment of the bond anharmonicity and on the Peierls-Boltzmann equation (PBE) treatment of quasi-particle transport described below, have worked well in capturing phonon dispersions, heat capacity, thermal expansion and thermal conductivity of weakly anharmonic systems.

However, in the case of strongly anharmonic materials such as alkali halides and heavy-

metal chalcogenides, the conventional lowest-order perturbative treatment of the bond anharmonicity can be insufficient [16–25]. Furthermore, the PBE theory of phonon transport relies on the presence of well-defined quasi-particles, whose mutual collision frequencies (Γ) must be significantly smaller than their vibrational frequencies (ω), i.e., $\Gamma \ll \omega$ [25, 26]. This condition could be violated in strongly anharmonic materials. Allen [25] estimated that it is safe to use the conventional quasi-particle theory if the thermal conductivity (k) is larger than k_{min} around $5\Theta_D/300\ Wm^{-1}K^{-1}$, where Θ_D is the Debye temperature of the material. While for most weakly anharmonic materials like silicon and diamond this condition is comfortably satisfied well beyond room temperature, for many strongly anharmonic materials, the experimentally measured k is close to, or even lower than, k_{min} even at room temperature, calling into question the validity of the conventional PBE treatment of phonon transport.

In this work, we demonstrate that, in fact, the conventional theory fails dramatically in describing the thermal properties of highly anharmonic materials. As an example crystal, we examine sodium chloride (NaCl), which is a strongly anharmonic compound with weak ionic bonds and is representative of a wide class of similar strongly anharmonic materials. We show that the conventional first-principles theory significantly over-predicts bond anharmonicity, and as a result gives phonon frequencies, thermal expansion and thermal conductivity that are in poor agreement with measured data. It also becomes inapplicable at relatively low temperature due to the complete breakdown of the quasi-particle picture.

To address these failures, we have developed a unified first-principles approach using many-body physics to describe thermal properties of insulating crystals within the same theoretical framework. The theory is applicable across the full range of bonding anharmonicity spanning low to high temperatures, and weakly-bonded to strongly-bonded materials. A central feature of this theory is a new *ab initio* phonon renormalization scheme based on many-body perturbation theory, from which well-defined quasi-particles emerge over the entire temperature range considered in this work. Furthermore, we show that higher-order four-phonon interactions, beyond the conventional lowest-order three-phonon processes, are required to simultaneously capture both the magnitudes and the temperature dependence of the experimentally measured thermal conductivity in NaCl. The new approach demon-

strates good agreement with experiments for phonon dispersions, thermal conductivity and thermal expansion of NaCl *simultaneously*, which rigorously confirms the validity of the quasi-particle theory for the renormalized phonons. Finally, we show that our renormalization framework, along with four-phonon scattering, also successfully predicts the measured phonon properties of a weakly anharmonic material - diamond, indicating universal applicability for thermal properties of insulators. The first-principles approach developed here should have wide applicability to several classes of highly anharmonic materials, where the conventional quasi-particle theory is likely to fail.

II. PHONONS, THERMAL EXPANSION AND THERMAL CONDUCTIVITY: CONVENTIONAL THEORY

We begin our analysis by briefly describing the conventional first-principles procedure to calculate phonon and thermal properties of semiconductors and insulators. Here we use the word "conventional" to describe widely used approaches in the literature, which are based on the lowest order perturbative treatment of the bond anharmonicity, without considering any higher-order effects, i.e. they do not include phonon renormalization or higher-order phonon-phonon scattering. Phonons, their temperature dependence, and their mutual interaction are described through the inter-atomic potential, Φ, which can be separated as $\Phi = \Phi_0 + \Phi_H + \Phi_A$, where Φ_0 is the energy of the lattice atoms in their equilibrium positions, and Φ_H and Φ_A are the harmonic (second-order) and anharmonic (third-order and beyond) energies for the displacement of atoms from their equilibrium positions, respectively. Φ_A can be expressed in a perturbative expansion in successively higher-orders of the atomic displacement: $\Phi_A = \Phi_3 + \Phi_4 + \ldots$. In a similar way, the Helmholtz free energy, from which the lattice parameters, $\{a_i\}$, are determined, can be separated as $F = \Phi_0 + F_H + F_A$, where F_H and F_A give the harmonic and anharmonic parts, and $F_A = F_3 + F_4 + \ldots$ is also expressed as perturbative expansion. The procedure to calculate the harmonic (Φ_H) and anharmonic (Φ_A) potential energies from first-principles, and explicit expressions for the harmonic (F_H) and anharmonic (F_A) free energies are given in Appendices A and B respectively.

Phonons

The conventional first-principles approach to calculate phonon modes is accomplished within the harmonic approximation, where $\Phi = \Phi_0 + \Phi_H$. Then, Φ_0 alone is minimized with respect to the lattice parameters for the crystal being examined, within the framework of density functional theory (DFT). Second-order inter-atomic force constants (IFCs) are calculated and used to construct the dynamical matrix, from which phonon modes are calculated (see Appendix A). At this level, there is no thermal expansion, i.e. $\{\partial a_i/\partial T\} = 0$, since Φ_0 does not depend on T. Furthermore, the anharmonic contribution (Φ_A) to the inter-atomic potential is ignored for the calculation of phonon frequencies and eigenvectors. Henceforth, we call these phonons, the *bare* phonons.

Thermal expansion

In the conventional theory, thermal expansion is typically included within the framework of the *quasi-harmonic* approximation (QHA) [27]. In the QHA, F is approximated as: $F_{\rm QHA}\left(\{a_i\}, T\right) \approx \Phi_0\left(\{a_i\}\right) + F_H\left(\omega\left(\{a_i\}\right), T\right)$, where $\omega\left(\{a_i\}\right)$ are the phonon frequencies calculated from DFT at each of the lattice parameters, $\{a_i\}$. Henceforth, we call these phonons, the *quasi-harmonic* (QH) phonons. The lattice parameters are now functions of T because phonon frequencies are taken to be functions of the $\{a_i\}$. Thermal expansion of the lattice, $\{a_i\left(T\right)\}$, is determined by minimizing $F_{\rm QHA}$ at each temperature.

Lattice thermal conductivity

Within the conventional theory, the lattice thermal conductivity is calculated by solving the linearized Peierls-Boltzmann equation (PBE) for the non-equilibrium distribution function (n_λ) established from an assumed small temperature gradient, ∇T, across a sample:

$$\mathbf{v}_\lambda \cdot \nabla T \frac{\partial n^0_\lambda}{\partial T} = \left.\frac{\partial n_\lambda}{\partial t}\right|_{\rm collisions} \tag{1}$$

Here, $n^0_\lambda = 1/(e^{\hbar\omega_\lambda/(k_B T)} - 1)$ is the Bose distribution function for phonon mode, λ, with ω_λ and $\mathbf{v}_\lambda$ being the frequency and group velocity in that mode respectively. The intrinsic thermal resistance is introduced in the collision term from bare phonons interacting

through the lowest-order term in Φ_A i.e. Φ_3, which causes scattering events involving three-phonons [28, 29]. Here, the bare phonons and Φ_3 are calculated at the lattice constant that minimized Φ_0, and thus thermal expansion is ignored. Temperature enters only in describing phonon populations and three-phonon scattering rates. A more consistent approach, including thermal expansion effects, would be to solve the PBE using QH phonons and Φ_3 obtained within the QHA, although this is typically not done. Writing the non-equilibrium distribution function as $n_\lambda = n^0_\lambda + n^0_\lambda \left(n^0_\lambda + 1\right) \mathbf{F}_\lambda \cdot (-\nabla T)$ gives an equation for the vector function $\mathbf{F}_\lambda$ [9–15, 30, 31]:

$$\mathbf{F}_\lambda = \mathbf{F}^0_\lambda + \tau^{(3\text{ph+iso})}_\lambda \left\{ \sum_{\lambda_1 \lambda_2} \left[W^{(+)}_{\lambda\lambda_1\lambda_2} \left(\mathbf{F}_{\lambda_2} - \mathbf{F}_{\lambda_1}\right) + \frac{1}{2} W^{(-)}_{\lambda\lambda_1\lambda_2} \left(\mathbf{F}_{\lambda_2} + \mathbf{F}_{\lambda_1}\right) \right] + \sum_{\lambda_1} W^{\text{iso}}_{\lambda\lambda_1} \mathbf{F}_{\lambda_1} \right\} \tag{2}$$

In this equation, $1/\tau^{(3\text{ph+iso})}_\lambda = \sum_{\lambda_1\lambda_2} \left[W^{(+)}_{\lambda\lambda_1\lambda_2} + \frac{1}{2} W^{(-)}_{\lambda\lambda_1\lambda_2} \right] + \sum_{\lambda_1} W^{\text{iso}}_{\lambda\lambda_1}$ is the three-phonon scattering rate from mode λ, $W^{(\pm)}_{\lambda\lambda_1\lambda_2}$ are scattering probabilities involving the three phonon modes, λ, λ_1 and λ_2, $W^{\text{iso}}_{\lambda\lambda_1}$ are the phonon-isotope scattering probabilities, and $\mathbf{F}^0_\lambda = \hbar\omega_\lambda \mathbf{v}_\lambda \tau^{(3\text{ph+iso})}_\lambda / k_B T^2$ with k_B being the Boltzmann constant. Full solution of the PBE properly accounts for the difference between momentum-conserving Normal and resistive Umklapp scattering processes [28, 29]. Retaining only the first term in the PBE (just $\mathbf{F}^0_\lambda$) gives the relaxation time approximation (RTA), which incorrectly treats the Normal processes as directly resistive [28, 29]. Expressions for these quantities are given in the Appendix B. Solution of the PBE then gives the thermal conductivity tensor, $k_{\alpha\beta}$, as:

$$k_{\alpha\beta} = \sum_\lambda C_\lambda v_{\lambda\alpha} F_{\lambda\beta} \tag{3}$$

where α and β are Cartesian components and $C_\lambda = (1/V)\, k_B \left(\partial n^0_\lambda / \partial T\right)$ is the volumetric heat capacity per mode.

III. FAILURE OF CONVENTIONAL THEORY FOR SODIUM CHLORIDE

The conventional first principles theory described in the previous section has done remarkably well at accurately describing phonon modes and thermal conductivities of dozens of compounds with no adjustable parameters (see, for example, Refs. [9–15]). To test the

ability of the conventional theory to capture the thermal properties of highly anharmonic materials, we have applied it to sodium chloride (NaCl), a weakly-bonded ionic crystal in the class of alkali halides with large thermal expansion and unusually low thermal conductivity, given its relatively light atoms. We have calculated the phonon dispersions, thermal expansion and lattice thermal conductivity using the conventional theory described in the previous section. For consistency in obtaining all three quantities within the same theory framework, we have used the QHA for all calculations, rather than (i) calculating phonons and thermal conductivity at the bare lattice constants and (ii) using the QHA for thermal expansion only. Furthermore, since our formulation determines anharmonic IFCs from thermally relevant finite temperature displacements (see Appendix A), these temperature-dependent unrenormalized anharmonic IFCs (along with the temperature-dependent unrenormalized harmonic IFCs from the quasi-harmonic approximation) are included in the thermal conductivity calculations of the above-described conventional approach. The results of our calculations using this conventional approach are shown in fig. 1.

Figure 1 (a) compares the calculated phonon dispersions to the measured INS data for NaCl [32]. The calculated optic phonon frequencies at 80 K and 300 K lie well below the corresponding measured values and show a softening with increasing temperature, while the INS measurements show almost no temperature dependence. This is particularly evident for the transverse optic (TO) phonon branch. Also, as shown in Fig. 1 (b), the NaCl lattice parameters calculated in the QHA increase much faster with temperature than do the measured values above 300 K [33–36], giving much larger thermal expansion than measured experimentally. In contrast, the lattice thermal conductivity calculated in the QHA, limited by lowest order three-phonon and phonon-isotope scattering, $k_3^{(\mathrm{QHA})}$ (dashed black curve in Fig. 1 (c)), is in reasonably good agreement with the measured data [37–39]. Similar calculations in the literature [40, 41] also found reasonable agreement with measured data when including only lowest order three-phonon scattering. This is consistent with the good agreement found between the measured thermal conductivities for many materials and first-principles calculations that included only three-phonon scattering around and below room temperature [10–12, 14, 15].

The failure of the conventional theory to agree with experiments on phonon dispersion,

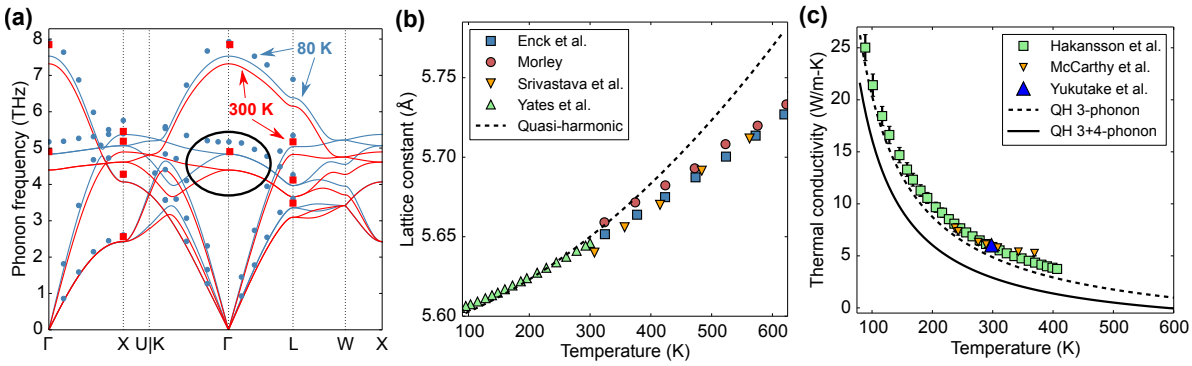

FIG. 1. **(a)** Calculated quasi-harmonic phonon dispersions compared with measured data from Raunio et al [32] at 80 K (blue) and 300 K (red). Circled region shows transverse optic (TO) branch near Γ. **(b)** Rate of thermal expansion calculated in the QHA (dashed black curve) compared with measured data [33–36]. **(c)** Three-phonon and 3+4-phonon limited thermal conductivity as a function of temperature calculated using quasi-harmonic phonons compared with measured data from Hakansson et al. [37] (extrapolated from low pressure values), McCarthy et al. [38] and Yukutake et al. [39].

thermal expansion and thermal conductivity of NaCl *simultaneously*, presents a problem. A consistent theory of thermal properties should be able to capture all of the above quantities within the same framework. The failure of the conventional theory to do so means that the QHA is inadequate for NaCl. This suggests that the perturbative treatment of anharmonicity about the phonons calculated in the QHA is breaking down, resulting in stronger apparent anharmonicity than observed experimentally, manifested by excessive phonon softening and too large thermal expansion.

Although the thermal conductivity calculations within the QHA including only three-phonon scattering agrees with the measured data for NaCl, inclusion of higher-order phonon-phonon scattering - that between four phonons, will necessarily reduce the calculated thermal conductivity below the measured value. Since the perturbative treatment is breaking down for NaCl due to the strong apparent anharmonicity described earlier, inclusion of four-phonon scattering should significantly worsen the agreement of the calculated thermal conductivity ($k_{3+4}^{(\mathrm{QHA})}$) with experiments. To test this proposition, we have included

four-phonon scattering in the solution of the PBE (Eq. 2), which transforms into:

$$\mathbf{F}_\lambda = \mathbf{F}^0_\lambda + \tau^{(\mathrm{tot})}_\lambda \sum_{\lambda_1\lambda_2} \Bigg\{ \left[W^{(+)}_{\lambda\lambda_1\lambda_2} \left(\mathbf{F}_{\lambda_2} - \mathbf{F}_{\lambda_1}\right) + \frac{1}{2} W^{(-)}_{\lambda\lambda_1\lambda_2} \left(\mathbf{F}_{\lambda_2} + \mathbf{F}_{\lambda_1}\right) \right] + \sum_{\lambda_1} W^{\mathrm{iso}}_{\lambda\lambda_1} \mathbf{F}_{\lambda_1} + \sum_{\lambda_1\lambda_2\lambda_3} \Bigg[\frac{1}{6} Y^{(1)}_{\lambda\lambda_1\lambda_2\lambda_3} \left(\mathbf{F}_{\lambda_1} + \mathbf{F}_{\lambda_2} + \mathbf{F}_{\lambda_3}\right) + \frac{1}{2} Y^{(2)}_{\lambda\lambda_1\lambda_2\lambda_3} \left(\mathbf{F}_{\lambda_2} + \mathbf{F}_{\lambda_3} - \mathbf{F}_{\lambda_1}\right) + \frac{1}{2} Y^{(3)}_{\lambda\lambda_1\lambda_2\lambda_3} \left(\mathbf{F}_{\lambda_3} - \mathbf{F}_{\lambda_2} - \mathbf{F}_{\lambda_1}\right) \Bigg] \Bigg\} \tag{4}$$

Equation 4 is changed in two ways compared to the three-phonon PBE of Eq. 2. First, the scattering rates now include both three-phonon and four-phonon scattering, along with phonon-isotope scattering: $1/\tau^{(\mathrm{tot})}_\lambda = 1/\tau^{(\mathrm{3ph+iso})}_\lambda + 1/\tau^{(\mathrm{4ph})}_\lambda$ where $1/\tau^{(\mathrm{4ph})}_\lambda = \sum_{\lambda_1\lambda_2\lambda_3} \left[\frac{1}{6} Y^{(1)}_{\lambda\lambda_1\lambda_2\lambda_3} + \frac{1}{2} Y^{(2)}_{\lambda\lambda_1\lambda_2\lambda_3} + \frac{1}{2} Y^{(3)}_{\lambda\lambda_1\lambda_2\lambda_3} \right]$, with $Y^{(1)}_{\lambda\lambda_1\lambda_2\lambda_3}$, $Y^{(2)}_{\lambda\lambda_1\lambda_2\lambda_3}$ and $Y^{(3)}_{\lambda\lambda_1\lambda_2\lambda_3}$ being scattering probabilities for the different four-phonon processes, as described in the Appendix B. Second, the last term in Eq. 4 is new. It conveys the distinction between Normal and Umklapp processes for four-phonon scattering. Without it, four-phonon scattering would be treated within the RTA, as has been done previously [42]. Computation of the four-phonon scattering probabilities and the iterative solution of Eq. 4 are challenging tasks which require extremely large computation time and storage memory. We have developed a number of computational efficiencies to obtain the 3+4-phonon limited thermal conductivity by fully solving Eq. 4, as summarized in Appendix D.

We calculated the lattice thermal conductivity of NaCl including three-phonon scattering, four-phonon scattering and phonon-isotope scattering within the QHA, $k^{(\mathrm{QHA})}_{3+4}$. The result is shown by the solid black curve in Fig. 1 (c). $k^{(\mathrm{QHA})}_{3+4}$ lies well below the measured data [37–39] over the full range of temperatures (100 K - 400 K). For example, it is 20% below the lowest value (extrapolated from low pressure measurements) from Ref. [37] at 100 K and almost 60% below it at 400 K. We also calculated the 3+4-phonon and phonon-isotope scattering limited thermal conductivity from 100 K - 600 K, using the lattice constants and IFCs (harmonic and anharmonic) calculated at a low temperature of 80 K, to mimic the conventional approach without including any temperature dependence for the IFCs, phonon frequencies or lattice constants. The predicted three-phonon and 3+4-phonon limited thermal conductivities under this approximation also agree poorly with experiments both in magnitudes and temperature-dependent trends (see SI section S2 [43]).

Thus, the apparent success of the QHA with only three-phonon interactions, in accurately matching the measured lattice thermal conductivity of NaCl is in fact fortuitous, and the conventional perturbative treatment of the anharmonic bonds in NaCl fails to describe the measured phonon frequencies, the thermal expansion and the thermal conductivity.

We have traced these failures to the unusually strong anharmonicity in the ionic bonds of NaCl, which invalidates the perturbative anharmonic expansion for the quasi-harmonic (QH) phonons and even results in a breakdown of the quasi-particle picture beyond 400 K, on which the PBE relies. In order for quasi-particles to be well-defined, they must interact weakly, i.e., their vibrational frequencies (ω) must be significantly larger than the rates at which they scatter (Γ). This condition can be expressed mathematically as, $\Gamma \ll \omega$ [25, 26]. Figure 2 shows Γ_{3+4}/ω for the QH phonons of NaCl above 400 K, where Γ_{3+4} are the scattering rates including three- and four-phonon interactions. It is evident from Fig. 2 that in this temperature range, Γ_{3+4} are so large that over almost the whole frequency range the condition, $\Gamma \ll \omega$, is not satisfied for the QH phonons of NaCl. The breakdown at only 40% of the melting temperature of NaCl is surprising and is a signature of the extreme anharmonicity, which invalidates its perturbative treatment. Additionally, even though $\Gamma_{3+4} \ll \omega$ is satisfied in the range of 100 - 300 K, the breakdown of the quasi-particle picture at about 40% of the melting temperature, along with the poor experimental agreement of the phonon dispersion and 3+4-phonon limited thermal conductivity computed using QH phonons, indicates that the QH phonons over-predict phonon scattering in NaCl even between 100 K and 300 K.

IV. NOVEL PHONON RENORMALIZATION APPROACH

One of the approaches to overcome these problems is to renormalize the QH phonons into new quasi-particles that interact more weakly [16–25]. Previous efforts to obtain renormalized phonons have either fit effective second-order IFCs (from which phonons are calculated) to forces calculated using DFT [17–22] or include renormalization for phonon frequencies, admitting polarization mixing with some approximations [23, 24]. In this work, we have developed a new approach that explicitly renormalizes the second-order IFCs using a sta-

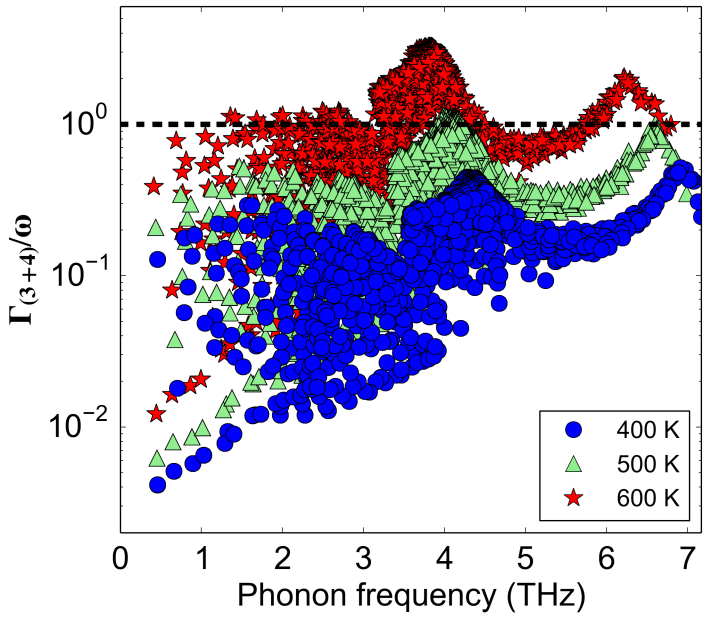

FIG. 2. Ratio of 3+4-phonon scattering rates to phonon frequency ($\Gamma_{(3+4)}/\omega$) calculated using quasi-harmonic phonons at three different temperatures. $\Gamma_{(3+4)}/\omega$ approaches 1 above 400 K and even exceeds it beyond $\sim$ 500 K, causing the quasi-particle description of the quasi-harmonic phonons to break down.

tistical perturbation-operator renormalization technique and many-body perturbation theory. Using this procedure, a new set of renormalized second-order IFCs ($\Theta_{jk}\left(N\nu, P\pi\right)$) are created from the bare (unrenormalized) second-order ($\Phi_{jk}\left(N\nu, P\pi\right)$) and fourth-order ($\Phi_{jklm}\left(N\nu, P\pi, Q\eta, R\rho\right)$) IFCs by solving the following equation:

$$\Theta_{jk}\left(N\nu, P\pi\right) = \Phi_{jk}\left(N\nu, P\pi\right) + \frac{\hbar}{4N_0}\sum_{QR}\sum_{\eta\rho}\sum_{lm}\sum_{\mathbf{q}s}\Phi_{jklm}\left(N\nu, P\pi, Q\eta, R\rho\right) \times \frac{W_l\left(\nu;\mathbf{q}s\right)W_m^*\left(\rho;\mathbf{q}s\right)}{\Omega_{\mathbf{q}s}\sqrt{M_\nu M_\rho}}e^{i\mathbf{q}\cdot\left(\mathbf{R}(Q)-\mathbf{R}(R)\right)}\left(2n_{\mathbf{q}s}+1\right) \quad (5)$$

where, $\Omega_{\mathbf{q}s}$ and $W_l\left(\nu;\mathbf{q}s\right)$ are the renormalized phonon frequencies and eigenvectors respectively of the phonon mode with wave vector $\mathbf{q}$ and polarization s, N, P, Q and R are the lattice sites, ν, π, ζ and ρ are the basis atom sites and N_0 is the number of lattice sites in the supercell (commensurate with the number of $\mathbf{q}$ points in the Brillouin zone). The derivation of the renormalization equation (Eq. 5) and extension of the renormalization to the anharmonic IFCs are detailed in Appendix C. Equation 5 shows that the renormalized

second-order IFCs ($\Theta_{jk}(N\nu, P\pi)$) depend on the renormalized phonon frequencies ($\Omega_{\mathbf{q}s}$, and therefore, the Bose factors $n_{\mathbf{q}s}$) and the renormalized phonon eigenvectors ($W_l(\nu; \mathbf{q}s)$), which in turn depend back on the renormalized second-order IFCs ($\Theta_{jk}(N\nu, P\pi)$). Therefore, Eq. 5 has to be solved self-consistently to obtain $\Theta_{jk}(N\nu, P\pi)$. To solve Eq. 5, the unrenormalized phonon frequencies ($\omega_{\mathbf{q}s}$) and eigenvectors ($w_l(\nu; \mathbf{q}s)$) are used as initial guesses and the renormalized second-order IFCs ($\Theta_{jk}(N\nu, P\pi)$) are updated at each iteration step.

A critical advantage of this approach is that since we renormalize the second-order IFCs directly, the renormalization seamlessly extends to the phonon frequencies, eigenvectors and group velocities. Furthermore, we can connect the changes to the phonon dispersions due to renormalization explicitly to one-phonon propagators, unlike some of the fitting approaches (see SI section S4 [43] for the relation between our renormalization procedure and the one-phonon propagator picture frequently used in many-body theory [24, 44–47]). Our approach is also able to capture the effects of zero-point motion, LO-TO splitting and finite temperature effects on the IFCs, which are particularly important for a polar, highly anharmonic material with relatively light atoms, like NaCl.

To apply the renormalization technique for NaCl, we first determine the unrenormalized IFCs on a two-dimensional grid of lattice parameters and temperatures, as described earlier. At each point on this grid, we perform the renormalization of the second, third and fourth-order IFCs. Next, we identify the lattice parameter that minimizes the anharmonic free energy including contributions out to fourth-order ($F = \Phi_0 + F_H + F_3 + F_4$, where F_H, F_3 and F_4 are defined in Appendix B) computed using the renormalized IFCs at each temperature, which also gives the thermal expansion directly. Inclusion of F_3 and F_4 is particularly important at elevated temperatures to accurately capture the thermal expansion, as shown in the SI section S1 [43]. Finally, we compute the phonon dispersion, three- and four-phonon scattering rates, and thermal conductivity using the renormalized IFCs by solving the 3+4-phonon PBE (Eq. 4) as for the QHA calculation.

V. PHONONS, THERMAL EXPANSION AND THERMAL CONDUCTIVITY: RENORMALIZATION APPROACH

The computed phonon dispersions obtained using the renormalization method show excellent overall agreement with the INS measurements [32] at both 80 K (Fig. 3 (a)) and 300 K (Fig. 3 (b)). In particular, the renormalized dispersions accurately capture the relative temperature independence of the optic phonons, consistent with the measured data [32]. In contrast, the QH phonon dispersions show significant softening between 80 K and 300 K.

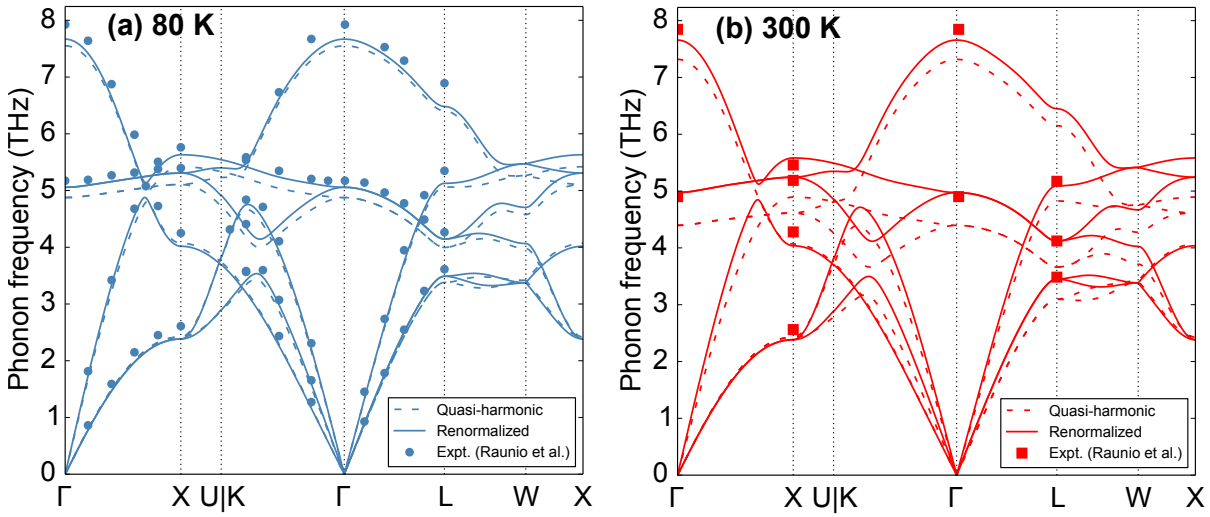

FIG. 3. Renormalized phonon dispersions at the fourth-order anharmonic free energy minimum lattice constants (solid curves), and phonon dispersions at the quasi-harmonic lattice constants (dashed curves) compared with measured data from Raunio et al [32] at **(a)** 80 K and **(b)** 300 K.

As shown in Fig. 4 (a), the experimental rate of thermal expansion [33–36] is also well captured by the renormalized anharmonic lattice parameters (solid black curve). In contrast, the lattice parameters calculated in the QHA (dashed curve) significantly over-predict the rate of thermal expansion. We note that the absolute values of the lattice parameters determined by the minimization of the QH and the renormalized anharmonic free energies were 0.9% and 0.5% larger than the room temperature experimental value of 5.645 ± 0.005 [33]. This is typical of under-bonding obtained from generalized gradient approximation-based

PBEsol exchange correlation functionals used for our DFT calculations. In order to compare the rate of thermal expansion with the measured data, we rigidly shifted both calculated curves in Fig. 4 (a) to match the experimental measurement only at 300 K. Interestingly, although both thermal expansion curves are similar in the range of 100 K to 300 K, the respective phonon dispersions (Fig. 3) show significantly different temperature-dependent behaviors.

We have confirmed that the renormalized phonons of NaCl satisfy the necessary condition to describe phonon transport using the PBE: $\Gamma_{3+4} \ll \omega$. Figure 4 (b) shows that Γ_{3+4} is much less than ω for the renormalized phonons even at a high temperature of 600 K, thereby enabling the Boltzmann treatment for phonon transport and thermal conductivity calculations over the entire temperature range considered in this work. Comparing to Fig. 2 for the QH phonons, a significant reduction in Γ_{3+4} is achieved through the renormalization process that gives well-defined quasi-particles.

Using the renormalized phonons and corresponding third- and fourth-order IFCs, we have calculated phonon-phonon scattering rates and lattice thermal conductivity. Figure 4 (c) shows that the three-phonon limited thermal conductivity calculated using renormalized phonons, k_3^{ren} (red dashed curve), is consistently larger than the measured data. The renormalized phonons have higher frequencies and interact more weakly than do the QH phonons. Including both three- and four-phonon scattering, k_{3+4}^{ren} (solid red curve) gives much better agreement with both the magnitudes and temperature dependence of the three different sets of experimental data [37–39]. This highlights that even with phonon renormalization, higher-order anharmonicity is required to capture the thermal conductivity of this strongly anharmonic material. We note that the slightly lower k_{3+4}^{ren} compared to the data is in part a consequence of the slightly larger lattice constant in our calculations compared to the measured value. For example, at 300 K, performing the calculations of k_{3+4}^{ren} at the measured lattice constant increases the calculated value by 7%, thereby improving the agreement with the measurements.

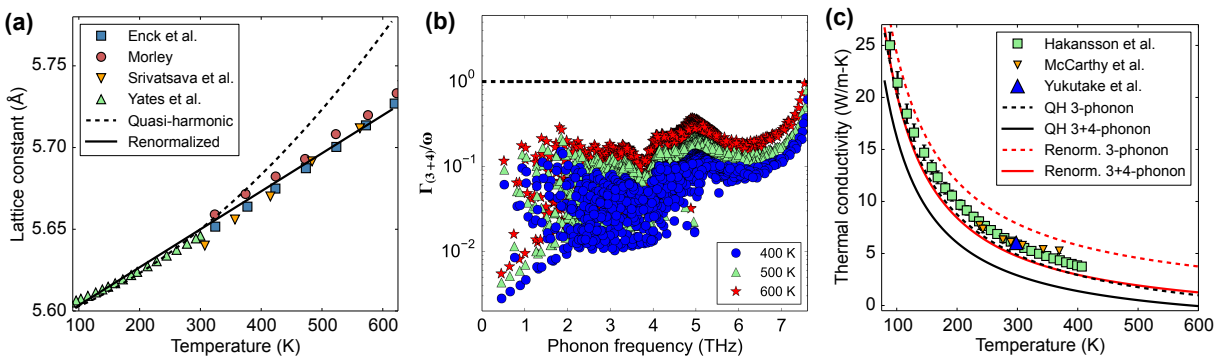

FIG. 4. **(a)** Rate of thermal expansion calculated in the QHA (dashed black curve) and by the phonon renormalization approach (solid black curve) compared with measured data [33–36]. **(b)** Ratio of 3+4 phonon scattering rates to phonon frequency ($\Gamma_{(3+4)}/\omega$) calculated using renormalized phonons at three different temperatures. The weakened scattering rates after phonon renormalization give a significant reduction to $\Gamma_{(3+4)}/\omega$ and produce well-defined quasi-particles. **(c)** Three-phonon and 3+4-phonon limited thermal conductivity as a function of temperature calculated using the renormalization approach (solid red curve) compared with measured data from Hakansson et al. [37], McCarthy et al. [38] and Yukutake et al. [39]. The corresponding curves (black) for the quasi-harmonic phonons are included for comparison.

VI. CANCELLATION OF ERRORS

For comparison, Fig. 4 (c) also includes the calculated k_3^{QHA} and k_{3+4}^{QHA} from Fig. 1 (c). Note that by coincidence, k_3^{QHA} is seen to overlap almost exactly with k_{3+4}^{ren}. On the other hand, the QH phonon dispersions (Fig. 3) and the rates of thermal expansion (Fig. 4 (a)) are significantly different between the two calculations. The main reason for the agreement between k_3^{QHA} and k_{3+4}^{ren} is a fortuitous cancellation of errors produced by strongly temperature dependent softening of the QH phonons and the neglect of four-phonon scattering processes in the QH calculation. Figure 5 show the temperature dependence of (a) QH and (b) renormalized phonons from 100 K to 600 K. The QH phonon modes soften significantly as the temperature is increased. Most importantly, the TO phonon branch softens by more than 1 THz between 100 K and 600 K, resulting in a substantial increase in the number of three-phonon scattering processes involving TO phonons as the temperature is increased, which gives stronger three-phonon scattering rates, and therefore mimics the measured stronger

temperature-dependent thermal conductivity trend at higher temperatures [37]. On the other hand, the renormalized phonon dispersions show a weaker temperature dependence, which results in weaker three-phonon scattering rates compared to the QHA calculations from 100 K-600 K. Experimental measurements are only recovered by including four-phonon scattering in the renormalized phonon calculations.

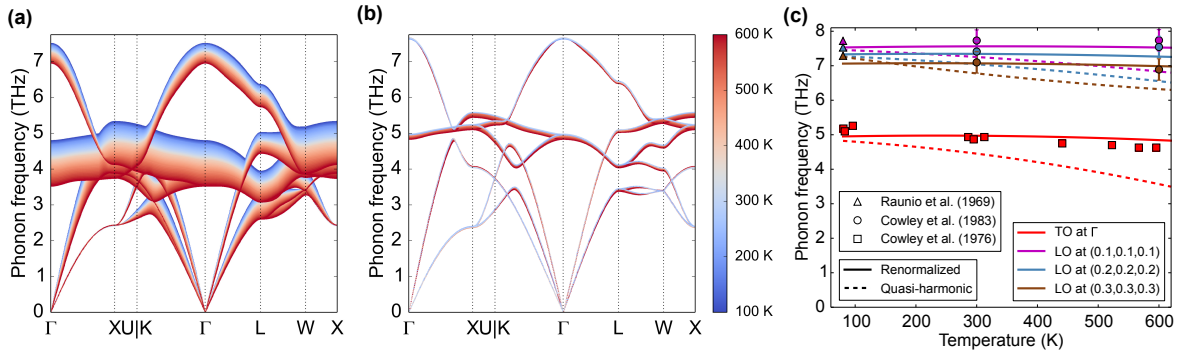

FIG. 5. Evolution of **(a)** quasi-harmonic and **(b)** renormalized phonon dispersions between 100 K and 600 K. **(c)** Temperature dependent phonon frequencies of the TO mode at Γ and the LO modes at $2\pi/a\,(0.1, 0.1, 0.1)$, $2\pi/a\,(0.2, 0.2, 0.2)$ and $2\pi/a\,(0.3, 0.3, 0.3)$ points in the Brillouin zone compared with INS [32, 48] and infra-red emission measurements [49]. The quasi-harmonic phonons show significant temperature driven softening while the renormalized phonon dispersions exhibit weak temperature dependence, consistent with the measured data [32, 48, 49].

The unusually weak temperature dependence of phonon modes in NaCl has also been observed in INS [32, 48] and infra-red emission measurements [49] for selected longitudinal optic (LO) and TO modes. As shown in Fig. 5 (c), the calculated renormalized phonons are in very good agreement with the measured weakly temperature-dependent TO mode frequencies at the Γ point and with the measured LO mode frequencies along the [111] direction from 100 K to 600 K, while the QH phonons show large softening and agree poorly with the experimental measurements [32, 48, 49].

To test the robustness of our results for NaCl, we have also performed the phonon renormalization and calculations of thermal expansion and $k^{\rm ren}_{3+4}$ for NaCl using a different pseudopotential with the exchange correlation under the local density approximation (LDA).

We find similarly good agreement between the magnitudes and temperature dependence of the renormalized phonons with the corresponding measured values. The calculated thermal expansion rate compares slightly worse to the measured data, while k_{3+4}^{ren} is in slightly better agreement with the data. We note however that the optimized LDA lattice constant is 5.5% lower than the measured value. (see SI section S5 [43] for the results of the LDA calculations).

VII. TEST FOR UNIVERSALITY: THE CASE OF DIAMOND

To test the universal applicability of our new first-principles approach, we performed the phonon renormalization, 3+4-phonon scattering and thermal conductivity calculations for diamond, a weakly anharmonic compound. We compared the calculated phonon dispersions (Fig. 6 (a)), thermal expansion (Fig. 6 (b)) and thermal conductivity (Fig. 6 (c)) with measured data and we find that:

1. The calculated bare and renormalized phonons are almost identical and give a very good match to the measured data [52–55].

2. The rate of thermal expansion calculated using QH and renormalized phonons are nearly identical for diamond and match well with the measurements [51]. The absolute value of the lattice constant at room temperature from our calculations is 3.5684 Å, which is within 0.1% of the experimental value [56]. The solid curve in Fig. 6 (b) was rigidly shifted to match the experimental value only at 300 K, similar to NaCl.

3. The calculated thermal conductivities accurately reproduce the measured data over a wide temperature range, as found previously [11, 42].

4. The differences between k_3^{QHA}, k_{3+4}^{QHA}, k_3^{ren} and k_{3+4}^{ren} are small until well above room temperature (Fig. 6 (d)).

Since the number of four-phonon scattering channels in diamond is much larger than that for three-phonon scattering, the obtained *null* result is a strong confirmation that the phonon renormalization approach and inclusion of higher-order anharmonicity is being captured accurately (see SI section S6 [43] for phonon dispersion and thermal conductivity calculations for diamond beyond 600 K). Thus our renormalization framework, along with four-phonon

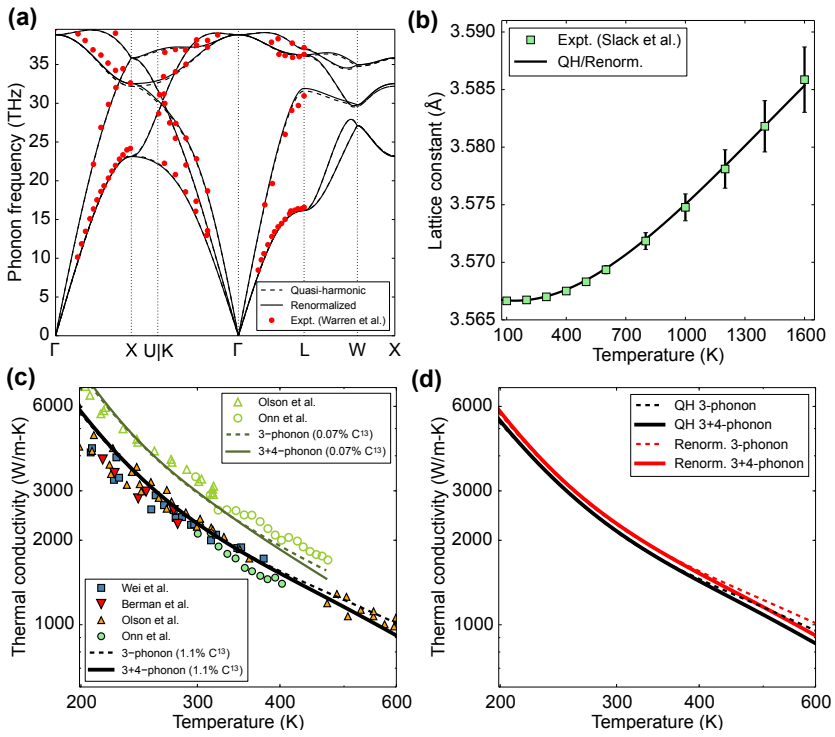

FIG. 6. **(a)** Quasi-harmonic (dashed curves) and renormalized phonon (solid curves) dispersions of diamond at 300 K compared with experiments from Warren et al. [50]. **(b)** Rate of thermal expansion as a function of temperature for diamond compared with measured data [51]. Both QH and renormalized phonons produce nearly identical thermal expansion rate. **(c)** Three-phonon (dashed curves) and 3+4-phonon (solid curves) limited thermal conductivity of diamond calculated using renormalized phonons and fourth-order free energy minimized lattice constant compared with experiments. The green curves are calculations for synthetic isotopically purified diamond with 0.07% C^{13} and the black curves are for naturally occurring diamond (1.1% C^{13}). The experiments are from Olson et al. [52](green empty triangles: synthetic isotopically purified diamond with 0.07% C^{13}, orange filled triangles: naturally occurring diamond with 1.1% C^{13}), Onn et al. [53](green empty circles: synthetic isotopically purified diamond with $< 0.05\%$ C^{13}, green filled circles: naturally occurring diamond with 1.1% C^{13}), Wei et al. [54](blue filled squares: naturally occurring diamond with 1.1% C^{13}) and Berman et al [55](red filled inverted triangles: naturally occurring diamond with 1.1% C^{13}). **(d)** Three-phonon (dashed curves) and 3+4-phonon (solid curves) limited thermal conductivity of diamond with quasi-harmonic (black) and renormalized (red) phonons.

scattering, is predictive for both weakly anharmonic (like diamond) and strongly anharmonic

(like NaCl) materials, indicating universal applicability for thermal properties of insulators.

VIII. CONCLUSIONS

In conclusion, we show that the conventional first-principles theoretical approach to calculate the thermodynamic and thermal transport properties for strongly anharmonic insulators fails because the perturbative treatment of anharmonicity using unrenormalized phonon modes is invalid. In such materials, the quasi-particle picture breaks down due to strong interactions between the unrenormalized phonons. In contrast, our newly developed first-principles approach accurately describes multiple thermal properties of both weakly anharmonic and strongly anharmonic insulators within the same theoretical framework. It features the following critical advantages:

1. *Phonon renormalization*: The novel phonon renormalization technique presented here, based on many-body perturbation theory, creates new well-defined quasi-particles and accurately describes the phonon and thermal transport properties of these materials.

2. *Four-phonon scattering*: For highly anharmonic materials or materials at high enough temperature, inclusion of higher-order phonon-phonon scattering in conjunction with phonon renormalization can be essential to accurately describe the phonon transport.

3. *Anharmonic Helmholtz free energy*: Use of the quasi-harmonic approximation for the Helmholtz free energy is inadequate for highly anharmonic materials. Inclusion of anharmonicity out to fourth-order shows improved agreement with measured thermal properties, particularly at high temperatures.

4. *Temperature-dependent inter-atomic force constants*: Temperature-dependent IFCs, calculated using thermally relevant displacements of atoms in our approach, closely represent the potential energy manifold ($\Phi(T)$) spanned by the atoms of the lattice at elevated temperatures (T). Furthermore, the effects of zero-point motion and polar LO-TO splitting effects on the displacement of atoms (and therefore, on the IFCs) is properly accounted for, in our approach. For highly anharmonic polar materials with light atoms, these effects become important even around room temperature.

Using the example of NaCl, a prototypical strongly anharmonic material with weak (ionic) bonds, we demonstrate that our new first-principles approach successfully recovers the experimentally observed thermal expansion, thermal conductivity and weak temperature dependence of phonon modes in NaCl simultaneously, which cannot be achieved using the conventional theory. We demonstrate that four-phonon scattering due to higher-order anharmonicity significantly affects both the magnitude and temperature dependence of the thermal conductivity of NaCl. Its inclusion is required to properly connect to the measured data. Furthermore, by computing the phonon and thermal properties of a weakly anharmonic material, diamond, we demonstrate that our first-principles framework is predictive for both weakly-bonded and strongly-bonded materials without any ad-hoc adjustments to the formulation, indicating universal applicability for thermal properties of insulators.

We expect the first-principles approach developed here to have wide applicability to several classes of highly anharmonic materials such as alkali halides, alkali and rare-earth hydrides and oxides, lead, bismuth and antimony chalcogenides, transition metal compounds and materials at high temperatures, in which the conventional theory of phonon properties and thermal transport has failed to serve as a predictive tool [4, 16–22, 24, 25, 57, 58].

Appendix A: Inter-atomic force constants from first-principles

To calculate the phonon and thermal properties described in the main text, we begin by expanding the potential energy as a sum of the equilibrium, harmonic and anharmonic contributions, given by:

$$\begin{aligned}\Phi = \Phi_0 &+ \underbrace{\frac{1}{2!}\sum_{NP}\sum_{\nu\pi}\sum_{ij}\Phi_{ij}\left(N\nu,P\pi\right)U_i\left(N\nu\right)U_j\left(P\pi\right)}_{\Phi_H} \\ &+ \underbrace{\frac{1}{3!}\sum_{NPQ}\sum_{\nu\pi\zeta}\sum_{ijk}\Phi_{ijk}\left(N\nu,P\pi,Q\zeta\right)U_i\left(N\nu\right)U_j\left(P\pi\right)U_k\left(Q\zeta\right)}_{\Phi_3} \\ &+ \underbrace{\frac{1}{4!}\sum_{NPQR}\sum_{\nu\pi\zeta\rho}\sum_{ijkl}\Phi_{ijkl}\left(N\nu,P\pi,Q\zeta,R\rho\right)U_i\left(N\nu\right)U_j\left(P\pi\right)U_k\left(Q\zeta\right)U_l\left(R\rho\right)+\ldots}_{\Phi_4}\end{aligned} \tag{A1}$$

Here, $\Phi_{ij}\left(N\nu, P\pi\right)$, $\Phi_{ijk}\left(N\nu, P\pi, Q\zeta\right)$ and $\Phi_{ijkl}\left(N\nu, P\pi, Q\zeta, R\rho\right)$ are the second, third and fourth-order inter-atomic force constants (IFCs) respectively, Φ_0 is the energy of the system in equilibrium, $N, P, Q, R, \ldots$ are the lattice sites, $\nu, \pi, \eta, \rho, \ldots$ are the labels for the basis atoms and $i, j, k, l, \ldots$ are the Cartesian indices. For this work, we truncate the Taylor series (Eq. A1) at Φ_4. In the conventional theory, the phonon frequencies and eigenvectors are obtained by diagonalizing the Fourier transform of second-order IFCs ($\Phi_{ij}\left(N\nu, P\pi\right)$) after scaling for the appropriate basis atom masses [59], and the three-phonon scattering probabilities are obtained using Fermi's Golden Rule (FGR) using the third-order IFCs ($\Phi_{ijk}\left(N\nu, P\pi, Q\zeta\right)$). For this work, we also calculate fourth-order IFCs ($\Phi_{ijkl}\left(N\nu, P\pi, Q\zeta, R\rho\right)$) to calculate four-phonon scattering probabilities from FGR.

The second-order IFCs are obtained from density functional perturbation theory (DFPT) using the Quantum ESPRESSO package [60]. The GBRV Ultrasoft pseudopotentials with PBEsol exchange correlation functional [61] were used for all calculations in this work, unless otherwise specified. For NaCl, a kinetic energy cutoff of 45 Ry for wave-functions, a kinetic energy cutoff of 200 Ry for charge density and potential, and a 4X4X4 Γ-shifted electronic $\mathbf{k}$-grid were found to provide total energy convergence of $< 3 \times 10^{-4}$ Ry and total stress convergence of < 0.3 kbar per unit cell. For the DFPT calculations, a 7X7X7 Γ-centered $\mathbf{q}$-grid provided converged phonon frequencies and eigenvectors. Similarly for diamond, a kinetic energy cutoff of 85 Ry for the wave-functions, a kinetic energy cutoff of 340 Ry for charge density and potential, and a 5X5X5 Γ-shifted electronic $\mathbf{k}$-grid were found to provide total energy convergence of $< 2 \times 10^{-5}$ Ry and total stress convergence of < 0.5 kbar per unit cell. For the DFPT calculations to obtain unrenormalized second-order IFCs and harmonic phonon properties, a 5X5X5 Γ-centered $\mathbf{q}$-grid for diamond provided converged bare phonon frequencies and eigenvectors.

To calculate the anharmonic (third and fourth-order) IFCs, we adopt a thermal stochastic snapshot technique based on the method described in Ref. [62]. In this technique, a 5X5X5 supercell is thermally populated with displacements according to the canonical ensemble. The temperature-dependent displacement of an atom at the N^{th} lattice site and the basis

site ν of the supercell is given by,

$$U_j\left(N\nu\right)=\frac{1}{\sqrt{M_\nu}}\sum_{\mathbf{q}s}\sqrt{\frac{\hbar\left(2n_{\mathbf{q}s}+1\right)}{\omega_{\mathbf{q}s}}}\cos\left(2\pi\zeta_{(1,\mathbf{q}s)}\right)\sqrt{-\log\left(1-\zeta_{(2,\mathbf{q}s)}\right)}w_j\left(\mathbf{q}s,\nu\right)e^{i\mathbf{q}\cdot\mathbf{R}(N)} \tag{A2}$$

where M_ν is the mass of the atom, $n_{\mathbf{q}s}$ is the Bose-Einstein distribution function, $\zeta_{(1,\mathbf{q}s)}$ and $\zeta_{(2,\mathbf{q}s)}$ are random variables providing mode-dependent "random kicks" to the total displacement of the atom $(N\nu)$. The two random numbers are constrained by: $\zeta_{(1,\mathbf{q}s)}=\zeta_{(1,-\mathbf{q}s)}$ and $\zeta_{(2,\mathbf{q}s)}=\zeta_{(2,-\mathbf{q}s)}$, so that the displacements $U_j\left(N\nu\right)$ in Eq. A2 are guaranteed to be real numbers. The displacements in Eq. A2 maintain the supercell at an average temperature T corresponding to the Bose factors $n_{\mathbf{q}s}$ under the canonical ensemble. Eq. A2 includes full quantum statistics including the zero-point motion (ZPM) of the atoms. Furthermore, in this work, we explicitly include the effects of LO-TO splitting on the displacements of atoms described in Eq. A2, which is important for highly polar materials like NaCl. The forces on atoms $(F_j\left(N\nu\right)=-\partial\Phi/\partial U_j\left(N\nu\right))$ due to the displacements $U_j\left(N\nu\right)$ were computed using density functional theory (DFT) and the Hellman-Feynman theorem using the Quantum ESPRESSO package. For these force-displacement calculations, the kinetic energy cutoffs remained the same as before, but a Γ-point and 1X1X1 Γ-shifted electronic $\mathbf{k}$-grid calculations provided convergences of $<10^{-5}$ Ry/au and $<5\times10^{-5}$ Ry/au for the forces in NaCl and diamond supercells respectively.

We fit the force-displacement dataset to Eq. A1 (after truncating to Φ_4) to extract the third and fourth-order IFCs. In practice, while fitting the IFCs, we subtract the total second-order contribution to forces (short-range evaluated using the DFPT second-order IFCs and the long-range as described in Ref. [63]) and only fit the anharmonic IFCs to the remaining forces. By enforcing point group symmetries and translational invariance conditions on the third and fourth-order IFCs, we identify and fit the force-displacement dataset to an irreducible set of anharmonic IFCs using a least-squares technique. All the reducible IFCs in Eq. A1 are replaced by linear combinations of the irreducible IFCs as determined by the point-group symmetry and translational invariance conditions. We perform the fitting procedure on a collection of thermal snapshots simultaneously and check for convergence of the IFCs with respect to the number of snapshots at each temperature. For NaCl, we required 75 snapshots at 100 K and 200 snapshots at 600 K to achieve a convergence of

< 0.01 eV/$\mathring{A}^3$ and < 0.01 eV/$\mathring{A}^4$ for the third and fourth-order IFCs respectively. For the same levels of convergence, we required 50 snapshots at 100 K and 100 snapshots at 750 K for diamond. The number of unknown irreducible IFCs to fit is always much smaller than the number of available force-displacement equations, thereby avoiding any over-fitting errors. For all of the calculations on NaCl, we employed second-order IFCs up to the eighth nearest neighbor, third-order IFCs up to the fifth nearest neighbor and fourth-order IFCs up to the third nearest neighbor, while for diamond, we employed second-order IFCs up to the tenth nearest neighbor, third-order IFCs up to the sixth nearest neighbor and fourth-order IFCs up to the third nearest neighbor. We did not observe any significant change in the specific heat, thermal conductivity and free energy while including one more shell of nearest neighbors for either second, third or fourth-order IFCs.

Appendix B: Expressions for free energy and phonon scattering probabilities

The expression for the Helmholtz free energy up to fourth-order is given by [64],

$$
\begin{aligned}
F_4 = \Phi_0 &+ \underbrace{\sum_{\mathbf{q}s}\left[\frac{1}{2}\hbar\omega_{\mathbf{q}s} + k_B T \log\left[1 - e^{-\hbar\omega_{\mathbf{q}s}/k_B T}\right]\right]}_{\mathrm{F_H}} \\
&+ \underbrace{\frac{1}{2}\sum_{\mathbf{q}s\mathbf{q}'s'} \Phi_{\mathbf{q}s,-\mathbf{q}s,\mathbf{q}'s',-\mathbf{q}'s'}\left(n_{\mathbf{q}s}+\frac{1}{2}\right)\left(n_{\mathbf{q}'s'}+\frac{1}{2}\right)}_{\mathrm{F_4}} \\
&\overbrace{-\frac{1}{2\hbar}\sum_{\mathbf{q}\mathbf{q}'\mathbf{q}'}\sum_{ss's''}\left(|\Phi_{\mathbf{q}s\mathbf{q}'s'\mathbf{q}''s''}|^2\left[\frac{n_{\mathbf{q}s}n_{\mathbf{q}'s'}+n_{\mathbf{q}s}+\frac{1}{3}}{\left(\omega_{\mathbf{q}s}+\omega_{\mathbf{q}'s'}+\omega_{\mathbf{q}''s''}\right)_p}+\frac{\left(2n_{\mathbf{q}s}n_{\mathbf{q}''s''}-n_{\mathbf{q}s}n_{\mathbf{q}'s'}+n_{\mathbf{q}''s''}\right)}{\left(\omega_{\mathbf{q}s}+\omega_{\mathbf{q}'s'}-\omega_{\mathbf{q}''s''}\right)_p}\right]\right.}^{\mathrm{F_3}} \\
&\left.+\,2\Phi_{\mathbf{q}s,-\mathbf{q}s,\mathbf{q}''s''}\Phi_{\mathbf{q}'s',-\mathbf{q}'s',-\mathbf{q}''s''}\frac{\left(n_{\mathbf{q}s}n_{\mathbf{q}'s'}+n_{\mathbf{q}s}+\frac{1}{4}\right)}{\left(\omega_{\mathbf{q}''s''}\right)_p}\right)
\end{aligned}
\tag{B1}
$$

where $\Phi_{\lambda\lambda_1\lambda_2} \equiv \Phi_{\mathbf{q}s\mathbf{q}'s'\mathbf{q}''s''}$ and $\Phi_{\lambda\lambda_1\lambda_2\lambda_3} \equiv \Phi_{\mathbf{q}s\mathbf{q}'s'\mathbf{q}''s''\mathbf{q}'''s'''}$ are the third-order and fourth-order matrix elements given by:

$$\begin{aligned}
\Phi_{\lambda\lambda_1\lambda_2} &= \Phi_{\mathbf{q}s,\mathbf{q}_1 s_1,\mathbf{q}_2 s_2} \\
&= (\hbar/2)^{3/2} \left(1/N_0^{1/2}\right) \left[\omega_{\mathbf{q}s}\omega_{\mathbf{q}_1 s_1}\omega_{\mathbf{q}_2 s_2}\right]^{-1/2} \\
&\quad \times \sum_{NP} \sum_{\mu\nu\pi} \sum_{\alpha\beta\gamma} \Phi_{\alpha\beta\gamma}\left(0\mu, N\nu, P\pi\right) \left(M_\mu M_\nu M_\pi\right)^{-1/2} \\
&\quad \times e^{i\mathbf{q}_1\cdot\mathbf{R}(N)} e^{i\mathbf{q}_2\cdot\mathbf{R}(P)} \\
&\quad \times w_\alpha\left(\mathbf{q}s,\mu\right) w_\beta\left(\mathbf{q}_1 s_1,\nu\right) w_\gamma\left(\mathbf{q}_2 s_2,\pi\right)
\end{aligned} \tag{B2}$$

and,

$$\begin{aligned}
\Phi_{\lambda\lambda_1\lambda_2\lambda_3} &= \Phi_{\mathbf{q}s,\mathbf{q}_1 s_1,\mathbf{q}_2 s_2,\mathbf{q}_3 s_3} \\
&= (\hbar/2)^2 \left(1/N_0\right) \left[\omega_{\mathbf{q}s}\omega_{\mathbf{q}_1 s_1}\omega_{\mathbf{q}_2 s_2}\omega_{\mathbf{q}_3 s_3}\right]^{-1/2} \\
&\quad \times \sum_{NPQ} \sum_{\mu\nu\pi\rho} \sum_{\alpha\beta\gamma\eta} \Phi_{\alpha\beta\gamma\eta}\left(0\mu, N\nu, P\pi, Q\rho\right) \left(M_\mu M_\nu M_\pi M_\rho\right)^{-1/2} \\
&\quad \times e^{i\mathbf{q}_1\cdot\mathbf{R}(N)} e^{i\mathbf{q}_2\cdot\mathbf{R}(P)} e^{i\mathbf{q}_3\cdot\mathbf{R}(Q)} \\
&\quad \times w_\alpha\left(\mathbf{q}s,\mu\right) w_\beta\left(\mathbf{q}_1 s_1,\nu\right) w_\gamma\left(\mathbf{q}_2 s_2,\pi\right) w_\eta\left(\mathbf{q}_3 s_3,\rho\right)
\end{aligned} \tag{B3}$$

Here, $\omega_{\mathbf{q}s}$ is the frequency of a phonon mode with wavevector $\mathbf{q}$ and polarization s, $w_\alpha\left(\mathbf{q}s,\mu\right)$ is the α^{th} component of the eigenvector of a phonon mode $(\mathbf{q}s)$ and for an atom at a basis site μ, and N_0 is the number of $\mathbf{q}$-points in the Brillouin zone.

The three-phonon scattering probabilities are given by,

$$\begin{aligned}
W^{(+)}_{\lambda\lambda_1\lambda_2} &= \frac{2\pi}{\hbar^2} \left|\Phi_{\lambda\lambda_1(-\lambda_2)}\right|^2 \left(n^0_{\lambda_1} - n^0_{\lambda_2}\right) \delta\left(\omega_\lambda + \omega_{\lambda_1} - \omega_{\lambda_2}\right) \\
W^{(-)}_{\lambda\lambda_1\lambda_2} &= \frac{2\pi}{\hbar^2} \left|\Phi_{\lambda(-\lambda_1)(-\lambda_2)}\right|^2 \left(1 + n^0_{\lambda_1} + n^0_{\lambda_2}\right) \delta\left(\omega_\lambda - \omega_{\lambda_1} - \omega_{\lambda_2}\right)
\end{aligned} \tag{B4}$$

and the four-phonon scattering probabilities are given by,

$$\begin{aligned}
Y^{(1)}_{\lambda\lambda_1\lambda_2\lambda_3} &= \frac{2\pi}{\hbar^2} \left|\Phi_{\lambda(-\lambda_1)(-\lambda_2)(-\lambda_3)}\right|^2 \frac{n^0_{\lambda_1} n^0_{\lambda_2} n^0_{\lambda_3}}{n^0_\lambda} \delta\left(\omega_\lambda - \omega_{\lambda_1} - \omega_{\lambda_2} - \omega_{\lambda_3}\right) \\
Y^{(2)}_{\lambda\lambda_1\lambda_2\lambda_3} &= \frac{2\pi}{\hbar^2} \left|\Phi_{\lambda\lambda_1(-\lambda_2)(-\lambda_3)}\right|^2 \frac{\left(1 + n^0_{\lambda_1}\right) n^0_{\lambda_2} n^0_{\lambda_3}}{n^0_\lambda} \delta\left(\omega_\lambda + \omega_{\lambda_1} - \omega_{\lambda_2} - \omega_{\lambda_3}\right) \\
Y^{(3)}_{\lambda\lambda_1\lambda_2\lambda_3} &= \frac{2\pi}{\hbar^2} \left|\Phi_{\lambda\lambda_1\lambda_2(-\lambda_3)}\right|^2 \frac{\left(1 + n^0_{\lambda_1}\right) \left(1 + n^0_{\lambda_2}\right) n^0_{\lambda_3}}{n^0_\lambda} \delta\left(\omega_\lambda + \omega_{\lambda_1} + \omega_{\lambda_2} - \omega_{\lambda_3}\right)
\end{aligned} \tag{B5}$$

where $\Phi_{\lambda\lambda_1\lambda_2}$ and $\Phi_{\lambda\lambda_1\lambda_2\lambda_3}$ are the three- and four-phonon matrix elements given by Eq. B2 and Eq. B3 respectively, and $-\lambda$ represents a phonon mode $((-\mathbf{q})\, s)$ when λ represents a phonon mode $(\mathbf{q}s)$. The phonon-isotope scattering probability is given by [65],

$$W^{\text{iso}}_{\lambda\lambda_1} = \frac{\omega^2_\lambda}{4N_0} \sum_b g_2\,(b)\, |\mathbf{w}\,(b,\lambda) \cdot \mathbf{w}^*\,(b,\lambda_1)|^2\, \delta\,(\omega_\lambda - \omega_{\lambda_1}) \tag{B6}$$

where, $g_2\,(b) = \left(1/\bar{M}_b^2\right) \sum_a f_{ab} \left(M_{ab} - \bar{M}_b\right)^2$ is a mass variance parameter with f_{ab} and M_{ab} being the concentration and mass of the a^{th} isotope of the b^{th} atom respectively and $\bar{M}_b$ is the average mass of the b^{th} atom. For all calculations on NaCl in this work, we used a natural isotopic mix of 75.76% of ^{35}Cl and 24.24% of ^{37}Cl for chlorine, while sodium is isotopically pure. For naturally occurring diamond, we used an isotopic mix of 98.93% of ^{12}C and 1.07% of ^{13}C. Quasimomentum conservation ($\mathbf{q} + \mathbf{q}_1 + \mathbf{q}_2 = \mathbf{G}$ for $\Phi_{\lambda\lambda_1\lambda_2}$ and $\mathbf{q} + \mathbf{q}_1 + \mathbf{q}_2 + \mathbf{q}_3 = \mathbf{G}$ for $\Phi_{\lambda\lambda_1\lambda_2\lambda_3}$, where $\mathbf{G}$ is a reciprocal lattice vector) is implied in the equations for the matrix elements (Eqs. B2 and B3). Energy conservation is treated computationally using the analytical tetrahedron scheme described in Ref. [66].

Appendix C: Renormalization of bare IFCs

The phonon renormalization in this work is achieved by renormalizing the bare second-order IFCs (determined from DFPT) using the anharmonic IFCs from Eq. A1. Renormalization of the phonon frequencies following the statistical perturbation operator-renormalization technique has been described in [64]. We extend this technique to derive self-consistent expressions for the renormalized second-order IFCs in terms of the practically computable quantities: renormalized phonon frequencies $\Omega_{\mathbf{q}s}$ and the renormalized eigenvectors $W_j\,(\mu; \mathbf{q}s)$.

For a system Hamiltonian $\mathcal{H} = KE + \Phi$, where KE is the kinetic energy and Φ is the potential energy, we define an effective harmonic potential Θ as:

$$\mathcal{H} = \underbrace{(KE + \Theta)}_{\mathcal{H}_H} + (\Phi - \Theta) \tag{C1}$$

where $\mathcal{H}_H$ is the purely harmonic effective Hamiltonian and $(\Phi - \Theta)$ is a correction term. Following Ref. [64], we can define renormalized creation and annihilation operators ($A^\dagger\,(\mathbf{q}s)$ and $A^\dagger\,(\mathbf{q}s)$ respectively) which satisfy the commutation relations:

$$\left[\mathcal{H}, A^\dagger\,(\mathbf{q}s)\right] = \hbar\Omega_{\mathbf{q}s} A^\dagger\,(\mathbf{q}s) + R^\dagger\,(\mathbf{q}s) \tag{C2}$$

where $R^{\dagger}(\mathbf{q}s) = \left[\Phi - \Theta, A^{\dagger}(\mathbf{q}s)\right]$ is a small remainder and $\hbar\Omega_{\mathbf{q}s}$ are the renormalized phonon frequencies corresponding to the effective harmonic potential Θ.

For any effective harmonic potential (Θ) and the corresponding phonon energies ($\hbar\Omega_{\mathbf{q}s}$), the remaining effective anharmonic potential ($\Phi - \Theta$) causes an anharmonic correction to the phonon energy, given by $\delta(\hbar\Omega_{\mathbf{q}s})$. The goal of the renormalization procedure is to make the correction, $\delta(\hbar\Omega_{\mathbf{q}s})$, as small as possible, so that the new quasi-particles, $\Omega_{\mathbf{q}s}$, weakly interact. To accomplish this, Ref. [64] constructs the renormalized effective second-order IFCs ($\Theta_{jk}(N\nu, P\pi)$) so that the contribution to $\delta(\hbar\Omega_{\mathbf{q}s})$ coming from the lowest order correction in $(\Phi - \Theta)$ vanishes. The expression for $\Theta_{jk}(N\nu, P\pi)$ obtained in Ref. [64] is given by,

$$\begin{aligned}\Theta_{jk}(N\nu, P\pi) &= \left\langle \frac{\partial^2 \Phi}{\partial U_j(N\nu)\, \partial U_k(P\pi)} \right\rangle \\ &= \Phi_{jk}(N\nu, P\pi) + \frac{1}{2} \sum_{QR} \sum_{\eta\rho} \sum_{lm} \Phi_{jklm}(N\nu, P\pi, Q\eta, R\rho) \left\langle U_l(Q\eta)\, U_m(R\rho) \right\rangle\end{aligned} \tag{C3}$$

where $\langle \cdot \rangle$ denotes the grand canonical thermal average. The third order term which would appear in Eq. C3 contains a factor $\langle U_m(R\rho) \rangle$, which vanishes since $\langle U_m(R\rho) \rangle = 0$.

Using the normal mode expansion for the displacement field ($U_j(N\nu)$) in terms of the renormalized phonon frequencies $\Omega_{\mathbf{q}s}$, the renormalized eigenvectors $W_j(\mu; \mathbf{q}s)$ and the normal mode coordinate ($\alpha(\mathbf{q}s)$), given by,

$$U_j(N\nu) = \frac{1}{\sqrt{N_0 M_\nu}} \sum_{\mathbf{q}s} \alpha(\mathbf{q}s)\, e^{i\mathbf{q}\cdot\mathbf{R}(N)} W_j(\nu; \mathbf{q}s) \tag{C4}$$

the thermal correlation average $\langle U_l(Q\eta)\, U_m(R\rho) \rangle$ is transformed into:

$$\left\langle U_l(Q\eta)\, U_m(R\rho) \right\rangle = \sum_{\mathbf{q}\mathbf{q}' ss'} \frac{W_l(\nu; \mathbf{q}s)\, W_m(\rho; \mathbf{q}'s')}{N_0 \sqrt{M_\nu M_\rho}} e^{i\mathbf{q}\cdot\mathbf{R}(Q) + i\mathbf{q}'\cdot\mathbf{R}(R)} \left\langle \alpha(\mathbf{q}s)\, \alpha(\mathbf{q}'s') \right\rangle \tag{C5}$$

The normal mode coordinates ($\alpha(\mathbf{q}s)$) can be written as:

$$\alpha(\mathbf{q}s) = \sqrt{\frac{\hbar}{2\Omega_{\mathbf{q}s}}} \left[A(\mathbf{q}s) + A^{\dagger}(-\mathbf{q}s) \right] \tag{C6}$$

Substituting Eq. C6 in Eq. C5, we get:

$$\langle U_l(Q\eta)\, U_m(R\rho)\rangle = \frac{\hbar}{2N_0}\sum_{\mathbf{q}\mathbf{q}'ss'}\frac{W_l(\nu;\mathbf{q}s)\, W_m(\rho;\mathbf{q}'s')}{\sqrt{M_\nu M_\rho}\sqrt{\Omega_{\mathbf{q}s}\Omega_{\mathbf{q}'s'}}}e^{i\mathbf{q}\cdot\mathbf{R}(Q)+i\mathbf{q}'\cdot\mathbf{R}(R)} \times\left\langle\left(A(\mathbf{q}s)+A^\dagger(-\mathbf{q}s)\right)\left(A(\mathbf{q}'s')+A^\dagger(-\mathbf{q}'s')\right)\right\rangle \tag{C7}$$

Now, it has been shown in Refs. [64, 67] that any arbitrary operator χ satisfies the following relation for the thermal correlation averages with the renormalized creation operator $A(\mathbf{q}s)$:

$$\langle\chi A(\mathbf{q}s)\rangle = \frac{\langle[A(\mathbf{q}s),\chi]\rangle}{e^{\hbar\Omega_{\mathbf{q}s}/k_BT}-1} \tag{C8}$$

Using the creation and annihilation operator commutation relations, we get:

$$\begin{aligned}\left\langle A^\dagger(\mathbf{q}'s')\, A(\mathbf{q}s)\right\rangle &= \frac{\delta_{\mathbf{q}\mathbf{q}'}\delta_{ss'}}{e^{\hbar\Omega_{\mathbf{q}s}/k_BT}-1} = n_{\mathbf{q}s}\delta_{\mathbf{q}\mathbf{q}'}\delta_{ss'}\\ \left\langle A(\mathbf{q}s)\, A^\dagger(\mathbf{q}s)\right\rangle &= \left\langle A^\dagger(\mathbf{q}s)\, A(\mathbf{q}s)\right\rangle + 1\\ \langle A(\mathbf{q}s)\, A(\mathbf{q}s)\rangle = \left\langle A^\dagger(\mathbf{q}s)\, A^\dagger(\mathbf{q}s)\right\rangle &= \left\langle A(\mathbf{q}s)\, A^\dagger(\mathbf{q}'s')\right\rangle = \left\langle A^\dagger(\mathbf{q}s)\, A(\mathbf{q}'s')\right\rangle = 0\end{aligned} \tag{C9}$$

Substituting Eqs. C9 into Eq. C7,

$$\begin{aligned}\langle U_l(Q\eta)\, U_m(R\rho)\rangle &= \frac{\hbar}{2N_0}\sum_{\mathbf{q}s}\frac{W_l(\nu;\mathbf{q}s)\, W_m^*(\rho;\mathbf{q}s)}{\Omega_{\mathbf{q}s}\sqrt{M_\nu M_\rho}}e^{i\mathbf{q}\cdot(\mathbf{R}(Q)-\mathbf{R}(R))}\\ &\quad\times\left(2\left\langle A^\dagger(\mathbf{q}s)\, A(\mathbf{q}s)\right\rangle+1\right)\\ &= \frac{\hbar}{2N_0}\sum_{\mathbf{q}s}\frac{W_l(\nu;\mathbf{q}s)\, W_m^*(\rho;\mathbf{q}s)}{\Omega_{\mathbf{q}s}\sqrt{M_\nu M_\rho}}e^{i\mathbf{q}\cdot(\mathbf{R}(Q)-\mathbf{R}(R))}(2n_{\mathbf{q}s}+1)\end{aligned} \tag{C10}$$

Substituting Eq. C10 into Eq. C3,

$$\Theta_{jk}(N\nu,P\pi) = \Phi_{jk}(N\nu,P\pi)+\frac{\hbar}{4N_0}\sum_{QR}\sum_{\eta\rho}\sum_{lm}\sum_{\mathbf{q}s}\Phi_{jklm}(N\nu,P\pi,Q\eta,R\rho) \times\frac{W_l(\nu;\mathbf{q}s)\, W_m^*(\rho;\mathbf{q}s)}{\Omega_{\mathbf{q}s}\sqrt{M_\nu M_\rho}}e^{i\mathbf{q}\cdot(\mathbf{R}(Q)-\mathbf{R}(R))}(2n_{\mathbf{q}s}+1) \tag{C11}$$

Equation C11 shows that the renormalized second-order IFCs ($\Theta_{jk}(N\nu,P\pi)$) depend on the renormalized phonon frequencies ($\Omega_{\mathbf{q}s}$, and therefore, the Bose factors $n_{\mathbf{q}s}$) and the renormalized phonon eigenvectors ($W_l(\nu;\mathbf{q}s)$), which in turn depend back on the renormalized second-order IFCs ($\Theta_{jk}(N\nu,P\pi)$). Therefore, Eq. C11 has to be solved self-consistently to obtain $\Theta_{jk}(N\nu,P\pi)$.

To solve Eq. C11 self-consistently, the bare phonon frequencies ($\omega_{\mathbf{q}s}$) and bare eigenvectors ($w_l(\nu;\mathbf{q}s)$) are used as initial guesses and the renormalized second-order IFCs ($\Theta_{jk}(N\nu,P\pi)$) are updated at each iteration step. Throughout the self-consistent iteration process, the bare second-order ($\Phi_{jk}(N\nu,P\pi)$) and fourth-order ($\Phi_{jklm}(N\nu,P\pi,Q\eta,R\rho)$) IFCs remain unchanged, for a given supercell force-displacement dataset. Creating new sets of thermal snapshots using renormalized IFCs and going through the entire cycle of (i) obtaining new sets of forces (ii) obtaining new sets of renormalized IFCs and (iii) calculating new k_{3+4}^{ren}, produced small changes in phonon dispersions, and $< 2.5\%$ change at 300 K and $\approx 5\%$ change at 600 K in k_{3+4}^{ren} (see SI section S7 [43] for details). Therefore, no additional DFT snapshot simulations are required other than the initial set of snapshots that provided the converged bare third-order and fourth-order IFCs, making this self-consistent solution technique computationally inexpensive. A critical advantage of this approach is that, since the second-order IFCs are renormalized, the renormalization seamlessly extends to the phonon frequencies, eigenvectors and group velocities without any ad-hoc adjustments to the formulation.

To obtain the renormalized third-order and fourth-order IFCs, we refit the same force-displacement dataset used earlier to a renormalized quartic potential energy model of the form:

$$\begin{aligned}\Phi = \Phi_0 &+ \frac{1}{2!}\sum_{NP}\sum_{\nu\pi}\sum_{ij}\Theta_{ij}(N\nu,P\pi)\,U_i(N\nu)\,U_j(P\pi)\\ &+ \frac{1}{3!}\sum_{NPQ}\sum_{\nu\pi\zeta}\sum_{ijk}\Psi_{ijk}(N\nu,P\pi,Q\zeta)\,U_i(N\nu)\,U_j(P\pi)\,U_k(Q\zeta) \qquad \text{(C12)}\\ &+ \frac{1}{4!}\sum_{NPQR}\sum_{\nu\pi\zeta\rho}\sum_{ijkl}\Psi_{ijkl}(N\nu,P\pi,Q\zeta,R\rho)\,U_i(N\nu)\,U_j(P\pi)\,U_k(Q\zeta)\,U_l(R\rho)\end{aligned}$$

$$F_i(N\nu) = -\frac{\partial\Phi}{\partial U_i(N\nu)} \qquad \text{(C13)}$$

Here, $\Theta_{ij}(N\nu,P\pi)$ are the renormalized second-order IFCs determined from Eq. C11 and $\Psi_{ijk}(N\nu,P\pi,Q\zeta)$ and $\Psi_{ijkl}(N\nu,P\pi,Q\zeta,Q\rho)$ are the renormalized third-order and fourth-order IFCs respectively. This final step of refitting the anharmonic IFCs is essential to ensure that the original set of force-displacement equations from DFT are still satisfied by the renormalized IFCs.

Appendix D: Computational efficiencies to mitigate cost

We have developed several computational efficiencies to mitigate the cost of obtaining the anharmonic IFCs and solving the 3+4-phonon PBE, without compromising accuracy. Notably,

1. To obtain the third and fourth-order IFCs, we have developed a thermal snapshot technique which requires only 100-200 DFT supercell calculations for each temperature. In contrast to this approach, the conventional supercell displacement technique [42] requires several hundreds to a few thousand DFT supercell calculations, making it prohibitively expensive for studying higher-order effects in thermodynamic and thermal transport properties. Moreover, the conventional supercell displacement technique cannot capture the effects of zero-point motion, polar effects/LO-TO splitting or the temperature dependence of the higher order IFCs, while our approach captures all of these effects at no additional cost.

2. The PBE for three and four-phonon scattering (Eq. 4) is solved on a grid of **q**-points in the Brillouin zone. The main challenge in the solution is the computation and storage of the four-phonon matrix elements ($\Phi_{\lambda\lambda_1\lambda_2\lambda_3}$). For example, even on a modest 17^3 **q**-grid, with six phonon polarizations in NaCl, 175 million three-phonon matrix elements ($\Phi_{\lambda\lambda_1\lambda_2}$) in the irreducible Brillouin zone for λ are calculated, while 5.2 trillion four-phonon matrix elements ($\Phi_{\lambda\lambda_1\lambda_2\lambda_3}$) in the irreducible λ grid are calculated, a factor of thirty-thousand larger. Furthermore, as shown in section S3 of the SI [43], both three-phonon and four-phonon scattering rates have a large contribution from Normal processes for NaCl. Since the RTA incorrectly treats Normal scattering processes as resistive, the solution of the PBE in the RTA will underestimate the thermal conductivity of NaCl. To avoid this problem, we solve the full 3+4-phonon PBE iteratively. Therefore, the four-phonon matrix elements used in Eq. 4 must not only be computed, but also stored in files for the subsequent iterations. Fortunately, since the tetrahedron scheme provides higher accuracy for the energy conservation than the commonly used adaptive Gaussian smearing scheme (see eg. Ref. [13]) or the non-adaptive Lorentzian scheme in Ref. [42], we obtain convergence at a much coarser phonon **q** grid density. For example, the 3+4-phonon limited thermal conductivity for

NaCl at 300 K obtained by solving Eq. 4 were different by only 1.6% between 17^3 and 21^3 phonon **q**-grid. Therefore, all the thermal conductivity results presented in this work were computed on a 17^3 **q**-grid. We also reduce the computational and storage costs significantly by first computing the four-phonon scattering phase space involving the energy conserving δ-functions for each $\lambda\lambda_1\lambda_2\lambda_3$ combination, and then computing and storing the matrix elements only for those processes which have a large enough phase space to contribute to Eq. 4.

AUTHOR CONTRIBUTIONS

N. K. R and D. B. originated the research idea. N.K.R. performed the first-principles calculations. N.K.R. and D.B. analyzed the data and wrote the manuscript. Both authors commented on, discussed and edited the manuscript.

ACKNOWLEDGEMENTS

This work was partially supported by Solid State Solar-Thermal Energy Conversion Center (S3TEC), an Energy Frontier Research Center funded by the U.S. Department of Energy, Office of Science, Office of Basic Energy Sciences under Award Number: DE-SC0001299/DE-FG02-09ER46577 (phonons and thermal expansion) and by the Office of Naval Research MURI, Grant No. N00014-16-1-2436 (thermal conductivity). We acknowledge the National Energy Research Scientific Computing Center (NERSC), a U.S. Department of Energy Office of Science User Facility operated under Contract No. DE-AC02-05CH11231, the Extreme Science and Engineering Discovery Environment (XSEDE), which is supported by National Science Foundation grant number ACI-1548562, and the Boston College linux clusters for the computational resources and support.

COMPETING INTERESTS

The authors declare no competing interests.

---

[1] B. Poudel, Q. Hao, Y. Ma, Y. Lan, A. Minnich, B. Yu, X. Yan, D. Wang, A. Muto, D. Vashaee, X. Chen, J. Liu, M. S. Dresselhaus, G. Chen, and Z. Ren, Science **320**, 634 (2008).

[2] M. Felderhoff and B. Bogdanovi, International Journal of Molecular Sciences **10**, 325344 (2009).

[3] X. Tang and J. Dong, Proceedings of the National Academy of Sciences **107**, 4539 (2010).

[4] O. Delaire, J. Ma, K. Marty, A. F. May, M. A. McGuire, M.-H. Du, D. J. Singh, A. Podlesnyak, G. Ehlers, M. D. Lumsden, and B. C. Sales, Nature Materials **10**, 614 (2011).

[5] D. S. Kim, O. Hellman, J. Herriman, H. L. Smith, J. Y. Y. Lin, N. Shulumba, J. L. Niedziela, C. W. Li, D. L. Abernathy, and B. Fultz, Proceedings of the National Academy of Sciences **115**, 1992 (2018).

[6] J. A. Johnson, A. A. Maznev, J. Cuffe, J. K. Eliason, A. J. Minnich, T. Kehoe, C. M. S. Torres, G. Chen, and K. A. Nelson, Phys. Rev. Lett. **110**, 025901 (2013).

[7] J. Callaway, Phys. Rev. **113**, 1046 (1959).

[8] R. A. Cowley, Reports on Progress in Physics **31**, 123 (1968).

[9] D. A. Broido, A. Ward, and N. Mingo, Phys. Rev. B **72**, 014308 (2005).

[10] D. A. Broido, M. Malorny, G. Birner, N. Mingo, and D. A. Stewart, Applied Physics Letters **91**, 231922 (2007).

[11] A. Ward, D. A. Broido, D. A. Stewart, and G. Deinzer, Phys. Rev. B **80**, 125203 (2009).

[12] L. Lindsay, D. A. Broido, and T. L. Reinecke, Phys. Rev. B **87**, 165201 (2013).

[13] W. Li, J. Carrete, N. A. Katcho, and N. Mingo, Computer Physics Communications **185**, 1747 (2014).

[14] A. Jain and A. J. McGaughey, Computational Materials Science **110**, 115 (2015).

[15] S. Lee, K. Esfarjani, J. Mendoza, M. S. Dresselhaus, and G. Chen, Phys. Rev. B **89**, 085206 (2014).

[16] R. Cowley, Advances in Physics **12**, 421 (1963).

[17] O. Hellman, I. A. Abrikosov, and S. I. Simak, Phys. Rev. B **84**, 180301 (2011).

[18] O. Hellman, P. Steneteg, I. A. Abrikosov, and S. I. Simak, Phys. Rev. B **87**, 104111 (2013).

[19] I. Errea, M. Calandra, and F. Mauri, Phys. Rev. Lett. **111**, 177002 (2013).

[20] P. Souvatzis, O. Eriksson, M. I. Katsnelson, and S. P. Rudin, Phys. Rev. Lett. **100**, 095901 (2008).

[21] A. van Roekeghem, J. Carrete, and N. Mingo, Phys. Rev. B **94**, 020303 (2016).

[22] G. A. S. Ribeiro, L. Paulatto, R. Bianco, I. Errea, F. Mauri, and M. Calandra, Phys. Rev. B **97**, 014306 (2018).

[23] T. Tadano and S. Tsuneyuki, Phys. Rev. B **92**, 054301 (2015).

[24] T. Tadano and S. Tsuneyuki, Journal of the Physical Society of Japan **87**, 041015 (2018).

[25] P. B. Allen, Phys. Rev. B **92**, 064106 (2015).

[26] G. Baym and L. P. Kadanoff, *Quantum statistical mechanics*, Vol. 1 (1962) p. 111.

[27] N. Mounet and N. Marzari, Phys. Rev. B **71**, 205214 (2005).

[28] R. E. Peierls, *Quantum theory of solids* (Oxford University Press, 1955).

[29] J. M. Ziman, *Electrons and phonons: the theory of transport phenomena in solids* (Oxford university press, 1960).

[30] M. Omini and A. Sparavigna, Physica B: Condensed Matter **212**, 101 (1995).

[31] M. Omini and A. Sparavigna, Phys. Rev. B **53**, 9064 (1996).

[32] G. Raunio, L. Almqvist, and R. Stedman, Phys. Rev. **178**, 1496 (1969).

[33] K. Srivastava and H. Merchant, Journal of Physics and Chemistry of Solids **34**, 2069 (1973).

[34] B. Yates and C. H. Panter, Proceedings of the Physical Society **80**, 373 (1962).

[35] G. L. Morley, The Journal of Chemical Physics **51**, 2336 (1969).

[36] F. D. Enck and J. G. Dommel, Journal of Applied Physics **36**, 839 (1965).

[37] B. Hakansson and P. Andersson, Journal of Physics and Chemistry of Solids **47**, 355 (1986).

[38] K. A. McCarthy and S. S. Ballard, Journal of Applied Physics **31**, 1410 (1960).

[39] H. Yukutake and M. Shimada, Physics of the Earth and Planetary Interiors **17**, 193 (1978).

[40] Y. Zhang, J. Dong, P. R. C. Kent, J. Yang, and C. Chen, Phys. Rev. B **92**, 020301 (2015).

[41] F. Zhou, W. Nielson, Y. Xia, and V. Ozoliņš, Phys. Rev. Lett. **113**, 185501 (2014).

[42] T. Feng, L. Lindsay, and X. Ruan, Phys. Rev. B **96**, 161201(R) (2017).

[43] "See Supplemental Material at [URL will be inserted by publisher] for more details on (1) free energy minimization, (2) calculations under the harmonic approximation, (3) importance of normal scattering, (4) relation between phonon renormalization in this work and one-phonon

propagators in many-body theory, (5) results with lda exchange correlation, (6) results for diamond at elevated temperatures and (7) convergence of the renormalization cycles.".

[44] G. D. Mahan, *Many-particle physics* (Springer Science & Business Media, 2013).

[45] G. Baym, Phys. Rev. **121**, 741 (1961).

[46] J. Kokkedee, Physica **28**, 374 (1962).

[47] A. A. Maradudin and A. E. Fein, Phys. Rev. **128**, 2589 (1962).

[48] E. R. Cowley, S. Satija, and R. Youngblood, Phys. Rev. B **28**, 993 (1983).

[49] E. R. Cowley, Journal of Physics C: Solid State Physics **5**, 1345 (1972).

[50] J. L. Warren, J. L. Yarnell, G. Dolling, and R. A. Cowley, Phys. Rev. **158**, 805 (1967).

[51] G. A. Slack and S. F. Bartram, Journal of Applied Physics **46**, 89 (1975).

[52] J. R. Olson, R. O. Pohl, J. W. Vandersande, A. Zoltan, T. R. Anthony, and W. F. Banholzer, Phys. Rev. B **47**, 14850 (1993).

[53] D. G. Onn, A. Witek, Y. Z. Qiu, T. R. Anthony, and W. F. Banholzer, Phys. Rev. Letters **68**, 2806 (1992).

[54] L. Wei, P. K. Kuo, R. L. Thomas, T. R. Anthony, and W. F. Banholzer, Phys. Rev. Letters **70**, 3764 (1993).

[55] R. Berman, P. R. W. Hudson, and M. Martinez, Journal of Physics C: Solid State Physics **8**, L430 (1975).

[56] S. Stoupin and Y. V. Shvyd'ko, Phys. Rev. B **83**, 104102 (2011).

[57] O. Hellman and D. A. Broido, Phys. Rev. B **90**, 134309 (2014).

[58] C. W. Li, X. Tang, J. A. Muñoz, J. B. Keith, S. J. Tracy, D. L. Abernathy, and B. Fultz, Phys. Rev. Lett. **107**, 195504 (2011).

[59] S. Baroni, S. de Gironcoli, A. Dal Corso, and P. Giannozzi, Rev. Mod. Phys. **73**, 515 (2001).

[60] P. Giannozzi, S. Baroni, N. Bonini, M. Calandra, R. Car, C. Cavazzoni, D. Ceresoli, G. L. Chiarotti, M. Cococcioni, I. Dabo, A. D. Corso, S. de Gironcoli, S. Fabris, G. Fratesi, R. Gebauer, U. Gerstmann, C. Gougoussis, A. Kokalj, M. Lazzeri, L. Martin-Samos, N. Marzari, F. Mauri, R. Mazzarello, S. Paolini, A. Pasquarello, L. Paulatto, C. Sbraccia, S. Scandolo, G. Sclauzero, A. P. Seitsonen, A. Smogunov, P. Umari, and R. M. Wentzcovitch, Journal of Physics: Condensed Matter **21**, 395502 (2009).

[61] K. F. Garrity, J. W. Bennett, K. M. Rabe, and D. Vanderbilt, Computational Materials Science **81**, 446 (2014).

[62] N. Shulumba, O. Hellman, and A. J. Minnich, Phys. Rev. B **95**, 014302 (2017).

[63] X. Gonze and C. Lee, Phys. Rev. B **55**, 10355 (1997).

[64] D. C. Wallace, *Thermodynamics of crystals* (Courier Corporation, 1998).

[65] S. Tamura, Phys. Rev. B **27**, 858 (1983).

[66] P. Lambin and J. P. Vigneron, Phys. Rev. B **29**, 3430 (1984).

[67] D. C. Wallace, Phys. Rev. **152**, 261 (1966).